X-ray measurement of intracellular chloride and other ions in mammalian cells

Gunawan, Renardi; Yang, Mengsu; Lau, Condon

Published in:
Talanta Open

Published: 01/08/2023

Document Version:
Final Published version, also known as Publisher's PDF, Publisher's Final version or Version of Record

Published version (DOI):
10.1016/j.talo.2023.100189

Publication details:
Gunawan, R., Yang, M., & Lau, C. (2023). X-ray measurement of intracellular chloride and other ions in mammalian cells. *Talanta Open*, *7*, [100189]. https://doi.org/10.1016/j.talo.2023.100189

Talanta Open 7 (2023) 100189

Contents lists available at ScienceDirect

Talanta Open

journal homepage: www.sciencedirect.com/journal/talanta-open

X-ray measurement of intracellular chloride and other ions in mammalian cells

Renardi Gunawan [a,b], Mengsu Yang [a,b], Condon Lau [c,*]

[a] Department of Biomedical Sciences, City University of Hong Kong, 83 Tat Chee Ave, Kowloon Tong, Hong Kong SAR PR China
[b] Tung Biomedical Sciences Centre, City University of Hong Kong, 83 Tat Chee Ave, Kowloon Tong, Hong Kong SAR PR China
[c] Department of Physics, City University of Hong Kong, 83 Tat Chee Ave, Kowloon Tong, Hong Kong SAR PR China

ARTICLE INFO

Keywords:
Intracellular ions
Chloride
Furosemide
X-Ray
Cell freeze-drying

ABSTRACT

Intracellular chloride ion (Cl^-) is known to have various roles in the cellular growth, modulation of cell cycles and volume, and in pathological disorders such as cancers, neurological and cardiovascular disorders. Various methods employed to measure intracellular Cl^- requires lengthy procedure and measurement duration, bulky and advanced instruments, or incapable to measure low to single-cell sample quantity. In this study, we report the measurement of intracellular chloride and other ions in mammalian cells using the FROZEN freeze-drying method for preparing adherent cell cultures for analysis. The sample preparation does not require chemical fixation and enables direct measurement by X-Ray analytical methods such as X-Ray Fluorescence (XRF) or Energy Dispersive X-Ray Fluorescence (EDS). Cell staining showed that the cells retained their content and location after preparation, which enables single-cell level analysis. Treatment of Furosemide to the cells disrupted the Cl^-, K^+ and Na^+ transport, causing changes in the intracellular ions. Additionally, the intracellular Cl^- of the dried cells was successfully measured, as low as 0.9 mM. The XRF and EDS measurements showed that treated cells displayed a significant reduction of intracellular Cl^- on all tested cell lines. However, no significant changes were detected in intracellular K^+. Furthermore, EDS analysis on single cells showed a significant decrease in intracellular Na^+ in most cell lines. These results demonstrate the efficiency and simplicity of the proposed method in intracellular ion analysis, allowing quick and simple preparation to measure biological samples with high sensitivity for various intracellular ions, which may be applicable in the diagnosis of diseases.

1. Introduction

Cellular homeostasis is the delicate balancing of ions within and around the cells, which is vital to maintaining their physiological functions [1]. Imbalances in intracellular ions could lead to impaired function and numerous diseases [2,3]. Alzheimer's [4] and cancers[5], for example, are known to have intracellular ion imbalance that further exacerbates the condition by accelerating cognitive dysfunction and associated with cancer growth and metastasis. Furthermore, manipulation of intracellular ions in cancer through the introduction of synthetic ion carriers is reported as a potential anticancer [6], displaying the importance of ion homeostasis for cells.

Chloride ion (Cl^-) is the most abundant anion in the cell. Cl^- is required to regulate nerve and muscle cells' excitability, preserve the cell's ionic composition, control cell volume, transport other ions across plasma membranes, and acidify lysosomes and other vesicles [7]. Moreover, Cl^- ion is reported to involve in cell proliferation, as blockage of Cl^- reduced cell growth [8]. Interestingly, Cl^- association with cell growth is not limited to normal cells but also cancer cells. Cl^- channel ClC-3 knockdown arrested nasopharyngeal carcinoma at G0/G1 phase, inhibited volume-activated Cl^- current and reduction of cell volume that correlated with cell growth [9,10]. Similar effect is reported in other cancers involving other Cl- channels as well [11–13]. Thus, the intracellular chloride ions in the cell show correlation to cancer growth and metastasis, making the intracellular Cl^- measurement could be applicable for cancer-related testing [11,14,15]. However, direct measurement of intracellular Cl^- poses several difficulties, mainly in relatively lower Cl^- ions transmembrane ratio and driving force in the cell [16].

Measurement of intracellular ions has been reported with various methods, utilizing chloride-sensitive electrodes [17,18], fluorescent dyes [19], nanoparticle probes [20–22], or patch clamp [23]. Microelectrode-based or microelectrometric titration measurement are

* Corresponding author.
E-mail address: Condon.lau@cityu.edu.hk (C. Lau).

https://doi.org/10.1016/j.talo.2023.100189
Received 7 December 2022; Received in revised form 19 January 2023; Accepted 25 January 2023
Available online 27 January 2023

capable to detect minute trace of Cl^- ions but requires a complex sample preparation and high number of cells, making it unsuitable for rapid measurement with low amount of sample. Moreover, electrode preparation demands a careful setting prior to measurement, which is time consuming, and electrode penetration may affect the cell's intracellular Cl^- condition [16,24]. Chloride-sensitive fluorescent dyes have high sensitivity but prone to bleaching, limiting the measurement duration. Additionally, leakage of the dyes from the cells were also reported [16, 25-27]. Lastly, intracellular Cl^- ions can be measured by genetic sensor produced by genetically modified cells through fluorescence or indirectly through the activity of enzymes related to intracellular Cl^-. The drawback of this method is the strenuous preparation steps needed to measure the intracellular Cl^- makes it unsuitable for diagnosis [28–30]. Moreover, fluorescence-based detection demands advanced instrumentations, further complicating the measurement [16].

NMR- and MRI-based Cl^- measurement provides a non-invasive method and doesn't involve ionizing radiation, thus allowing measurement on live cells with no risk of radiation damage. However, there are also drawbacks in using NMR, mainly its need to add shift reagent to distinguish the different source of ions, relatively expensive to perform and unable to be done in the field. Moreover, NMR measurement requires a strong magnetic field applied into the sample, affecting the surrounding area and severely limits the applicability of NMR-based ion detection [31]. Similarly, MRI-based Cl^- measurement requires powerful magnetic field to perform measurement, and on top of that, needs long scanning time. These hurdles inhibit their wider use for biological ion detection [32].

X-Ray fluorescence spectrometry (XRF) can rapidly determine ion components and their distribution in biological tissue samples [33,34]. Each ion emits distinct fluorescence when exposed to an X-Ray beam, thus enabling the detection of the ions within biological samples. This method has been employed to analyze plant cells, detect toxic ions (mercury, arsenic and other heavy metals) and trace element patterns associated with neurodegenerative diseases or other intracellular ions present in the cell [35–37]. XRF-based measurement is capable of measuring the intracellular ion in the sample directly, avoiding addition of dyes or probes to the samples. However, preparation of the samples for XRF analysis often includes chemical fixation, which may alter the cell ion concentrations for specific ions, as reported by Jin *et al.* (2016). The K^+ and Cl^- measured after chemical fixations step were significantly reduced (as low as 0.3% and 16% for K^+ and Cl^-, respectively) compared to the freezing method. Phosphorous (P) was also reported to be reduced after chemical fixation, demonstrating the efficiency of freezing-based cell preservation. The report utilizes the freeze-drying method but uses a complex and laborious cell-culturing method to prepare the cells and is only able to process a limited amount of cells due to the small area of cell culture [38]. Therefore, the development of a simple, low-cost and straightforward method to measure intracellular ions would facilitate rapid measurement of intracellular ions in biological samples.

In this report, we have optimized the method to measure intracellular ion with X-Ray based analysis. Several intracellular ions were measured after treatment of cells with chloride channel blocker Furosemide (FMD), a diuretic drug commonly used for treating hypertension and edema. FMD treatment could disrupt intracellular chloride balance by blocking Na^+-K^+−2Cl^-cotransporter (NKCC), one of the chloride ion transporters belonging to cation chloride cotransporters (CCC), through binding to the NKCC pore in the intracellular side and inhibit sodium, potassium, and chloride transfer across the cell membrane [39–41]. Inhibition of NKCC leads to lower intracellular Cl^- [42,43], which can be detected and quantified by X-Ray based methods XRF and EDS in combination with sample processing FROZEN method [44].

2. Experimental section

2.1. Materials

RPMI media (22400–089), DMEM media (11995–040), EpiLife™ medium (MEPI500CA) with growth supplement (EDGS) (S0125), Defined Keratinocyte-SFM Basal medium with growth supplement (107440109), Pen-Strep antibiotic (PS, 15140–122), fetal bovine serum (FBS, A3160801), TrypLE Express Enzyme (12604013) and phosphate-buffered saline (PBS, 10010–031) were purchased from ThermoFisher, USA. Furosemide (F4381) was purchased from Sigma Aldrich, USA. Potassium Chloride (KCl) was purchased from Sangon Biotech, China. Petri dishes used to culture cells were bought from Thermo, USA (150466). Sterile filters with 0.2 μm pores were purchased from Pall Corporation, USA (4612). Parafilm tape was purchased from Bemis, USA (PM-996).

2.2. Cell culture

SKOV3 ovarian cancer cell line (ATCC, HTB-77™) was cultured in RPMI media supplemented with 1% PS and 10% FBS. NP460 cell line was cultured in mixed media (1:1 ratio of EpiLife™ media supplemented with EDGS and Defined Keratinocyte SFM media with growth supplement) with 1% PS. A549 (ATCC, CCL-185™) and H1299 (ATCC, CRL-5803™) cell lines were cultured in DMEM media supplemented with 1% PS and 10% FBS. Cells were incubated until 80% confluence before dissociated for experiments

2.3. Preparation of 0.15 mg/mL FMD media

Furosemide stock was prepared by dissolving 15 mg of FMD in 500 μl DMSO to a final concentration of 0.3 mg mL^{-1}. FMD media was prepared by diluting FMD stock to 0.5% V/V with culture media. Afterward, the media was sterilized by filtering FMD media with a 0.2 μm sterile filter (Pall, USA) inside a biosafety cabinet.

2.4. Incubation of cells in FMD media

Cells were washed with PBS before dissociated from the culture flask with 1.5 mL TrypLE and centrifuged. Approximately 10,000 cells were then seeded in 10 cm Petri dishes with 10 mL complete media. All cell lines were seeded into Petri dishes with their respective media. After 24 h of incubation, culture media was replaced with 10 mL FMD media and incubated until reaching 95% confluence (4–6 days). The media was changed after 2 days of incubation with FMD media. Control cells were incubated with normal culture media and DMSO control cells were incubated with 0.5% DMSO + culture media.

2.5. Freeze-dried sample preparation

The freeze-dried cells were prepared based on a previously reported method, with some modifications [44]. All media in confluent Petri dishes was removed, and every dish was washed with PBS. Cells were washed by adding 10 mL MilliQ water to the dish while shaking the dish to make sure the MilliQ water covers the dish evenly, then immediately discarding the water. This process was repeated twice more, with the removal of the remaining water using a surgical pipette in the last washing step. The process should be performed quickly, approximately no more than 15 s from initial MilliQ washing to the end. Immediately afterward, each dish was exposed to liquid N_2 vapor for 30 s to freeze cells and moved to −80 °C fridge in frozen state. Each frozen dish was covered with parafilm, and small holes were punctured on parafilm. These samples were kept at −80 °C before being transferred to the freeze dryer (Labconco, USA) in frozen condition. The remaining frozen water on the dishes was removed by storage in a freeze dryer with 1 mBar or less pressure overnight. All samples were ensured to remain frozen

throughout freeze drying by adding small amounts of dry ice beneath each dish. The dried cells were recorded using a microscope with 40x magnification (Leica DMI300B, Germany).

2.6. Preparation of KCl spiked solution

The spiking solution was prepared based on calculations reported in a previous report [44]. Spiked solutions of KCl were prepared with the following assumptions:

1. Added concentration was calculated as per cell.
2. The amount of K^+ in the cells was approximately 100 mM.
3. On average, NP460 cells have 33.8 μm diameter, with cell volume of 1.62×10^{-10} L and will collapse to a small area of 897.25 μm^2.
4. Therefore, the K concentration in the area would be 1.8×10^{-12} mmol μm^{-2}.
5. To achieve those concentrations, solutions of corresponding salts with specific concentration needs to be dried to mimic a cell condition. For a 5 ml solution, if all liquid perfectly covers the entire Petri dish surface, the depth of the liquid will be 636.64 μm.
6. Assuming the volume of solution in a Petri dish is 636.64 μm, the required concentration for 5 mL salt solution will be 2.827 mmol L^{-1} for K.

2.7. KCl spiking preparation

Spiked cell samples were prepared by adding 5 mL of pre-cooled 5, 10, and 15 mM KCl solutions to freeze-dried cells. Samples were then stored at −80 °C immediately after addition for 30 mins, and then each dish was covered with parafilm and kept in frozen condition until placed in a freeze dryer machine. A small amount of dry ice was placed underneath the spiked dishes during freeze drying with a pressure of 1 mBar or lower overnight. Each KCl spiking was performed with 3 replicates, and the test was repeated 3 times.

2.8. XRF data acquisition and analysis

XRF measurement was done with Energy Dispersive X-Ray Fluorescence equipment Bruker S2 Puma (Bruker, USA) with 20 kV and Palladium (Pd) anode. The measurement was performed in vacuum condition with 60 s acquisition time. Dried cell samples in Petri dishes were cut into small chunks (less than 3 cm in width), and each sample was tested in 3 replicates from the same dish. Measurements were performed at 20 kV, and data analysis was done with normalization by the Palladium (Pd) spectrum peak. Each data on FMD treatments were calculated from at least 3 biological repeats with 3 replicates for each repetition. KCl spiking measurements were calculated from 3 biological repeats with 3 replicates for each repeat. Subsequent data was processed and compiled in Excel and GraphPad for statistical test and generation of graphs.

The concentration of Cl in cell lines were calculated by using the linear regression.

$$Y = ax + b$$

The intercept (a) and slope (b) was obtained from the KCl spiking experiment. The mean and SD of all normalized intensity for Cl in each cell lines (Y) were used to calculate the mM concentration of the sample (x). Since the line doesn't cross at 0 point in non-spiked sample (0 mM point), calibration was performed by reducing the numbers with x value if Y is 0. The calculation was performed on both mean and SD.

2.9. SEM-EDS data acquisition and analysis

Samples for the SEM-EDS test were prepared from dried cells in Petri dishes. The dishes were cut to a smaller size (roughly 0.5×0.5 cm^2) and mounted in the specimen holders by carbon tape. The samples were coated with carbon coating prior to SEM measurement. SEM-EDS test was performed with JEOL JSM IT500 Scanning Electron Microscope (JEOL, Japan) and operated at 15 kV in vacuum with 30 s acquisition time.

EDS analysis was done on a single cell level, with minimum 5 cells measured for each sample. Samples were collected from at least 2 different batches of dried cells for each cell line, totaling at minimum 10 cells measured per treatment in each cell line. The size of the scanned ROI varies from 30 to 40 μm^2. The EDS data was processed by AZtec software (Oxford Instruments, UK) and each result was normalized by the software. Subsequent data was processed and compiled in Excel and GraphPad for statistical test and generation of graphs.

2.10. Statistical analysis

Statistical analyses were performed using GraphPad Prism 8 software. Differences in XRF spectra intensity and EDS data throughout controls and FMD media treatment were assessed with one-way ANOVA with Tukey's multiple comparison test as post-Hoc test. Linear regressions of the spiking tests were calculated and displayed using GraphPad Prism 8.

3. Result and discussion

3.1. Cell freeze-drying

Cancer cell lines SKOV3, A549, H1299 and nasopharyngeal cell line NP460 were used in intracellular chloride ion (Cl^-) analysis using XRF and EDS. Dried cells were prepared by flash freezing of cultured cells after washing with dH_2O and then freeze-dried overnight under a vacuum (below 1 mBar). Dried cells displayed a relatively well-preserved morphology with minimal structural damage, and most cells remained fixed in their initial locations.

The cell freeze-drying method can maintain the location and preserve the cell membrane of most of the cells, which was confirmed by DAPI and calcein AM staining in dried cell analysis and further observed under SEM (Fig. 1). Most cells were seen intact, with some visible effect of dehydration on the cells (Fig. 1A). Cell stained with DAPI and calcein AM retained the dye after drying and displayed preserved cell morphology despite the shrinking due to dehydration. A side-by-side picture before and after cell drying (Fig. 1C and D) showed that most of the cell's nuclei were intact, while the cytoplasm shrunk and collapsed around the nuclei. Some cells were displaced during the washing and freeze-drying step, but most cells remained in the same place, confirming that the cell drying method could fix the cells into their locations for further analysis.

Under SEM (Fig. 1B, E-F), the same morphology can be observed on the dried cells. The nuclei were intact but deflated, and the cell membrane was fractured. Meanwhile, the cytoplasm was dried and collapsed, leaving behind tendril-shaped remains, due to lack of fixation step to preserve the cellular morphology prior to dehydration [45]. Furthermore, flattening of the nucleus is observed in fixed and non-fixed cells [46]. The cracks and crevices in the cell membrane are clearly shown in higher magnification, with some pores visible on the membrane (Fig. 1F).

Additionally, each cell line showed a distinct growth pattern under SEM (Supplementary figure S1), with NP460 and SKOV3 cells growing relatively close to each other in full confluency. In contrast, A549 grows in clusters and has small gaps in between the clusters, and H1299 grows in smaller clusters separated by small gaps. The dried cell morphology showed that the method successfully preserved the cells, as demonstrated in previous reports [38,44].

3.2. Intracellular ion analysis with XRF

After the cells were dried, several intracellular ions were measured with XRF. In total, 3 cancer cell lines (SKOV3, A549, H1299) and 1

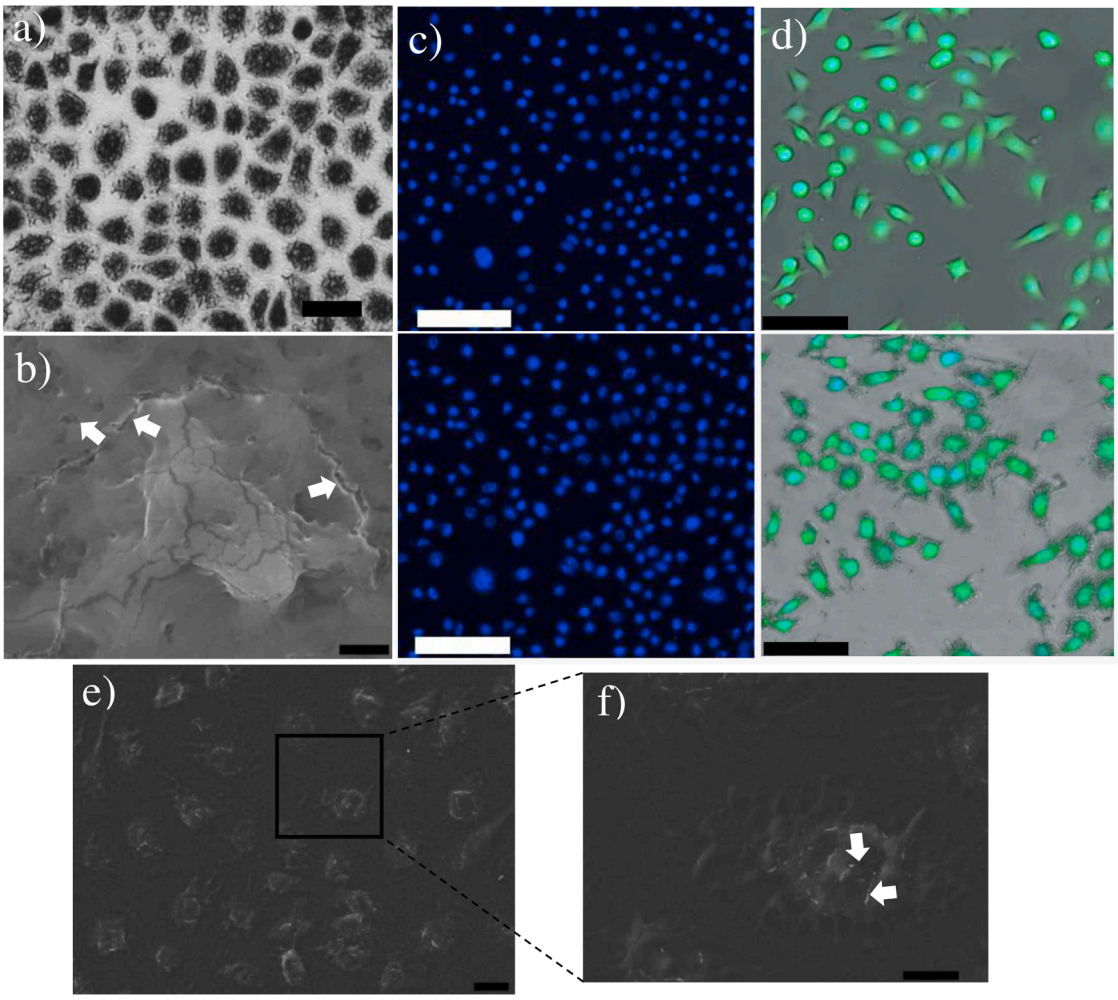

Fig. 1. The condition of post-treatment dried cells visualized under microscope. (A) Freeze-dried cells observed under brightfield. (B) Closer magnification (7000x) of dried cells with fissures in cell membrane pointed with arrows. Bar represents 50 and 2 μm. (C) DAPI and (D) Calcein AM stained cells on cells before being dried (top) and after being dried (bottom). Bars represent 100 μm. (E) Freeze-dried cells observed under SEM with 500x magnification. (F) The area within the insert is enlarged to 3000x magnifications. Bars represent 20 and 5 μm.

immortalized normal cell line (NP460) were subjected to Cl^- and K^+ analysis with XRF. Both normal and cancer cell lines were treated with FMD drug. As FMD drug is dissolved in DMSO, solvent control was added by incubating the cells with media with 0.5% DMSO to remove the effect of DMSO on the cells. The spectra obtained from XRF was normalized to Palladium (Pd) for instrumental control.

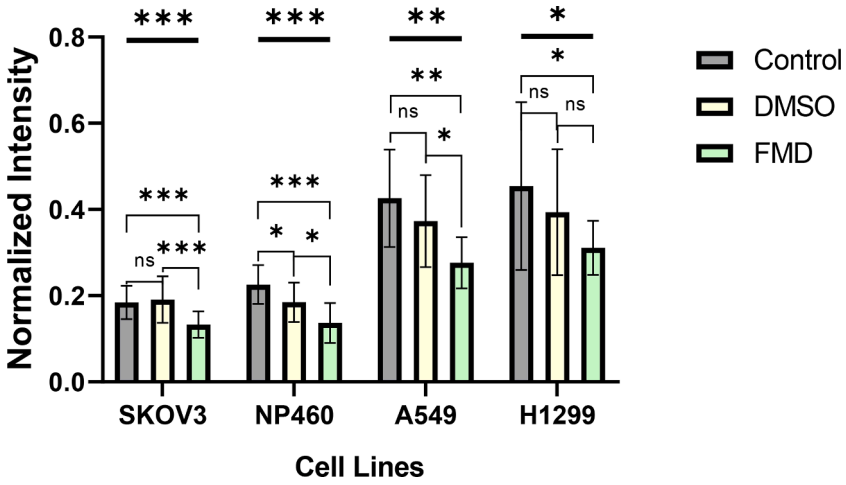

Fig. 2. XRF result of Cl^- measurement in dried cells with FMD treatment. Statistical tests were done with one-way ANOVA with Tukeys multiple comparison test. *: $P<0.05$, **: $P<0.01$, ***: $P<0.001$.

Treatment with FMD showed a significant reduction of intracellular Cl^- in all cell lines, as displayed in Fig. 2 below. DMSO control demonstrated a reduction of Cl^- in the majority of cell lines, though not as extensive as FMD treatment, which indicates the decline of Cl^- was not only caused by the FMD drug, but DMSO also influenced intracellular Cl^- reduction. The intracellular Cl^- reduction after treatment of FMD drug might be achieved through blocking of NKCC transporters that regulate the transport of Na^+, K^+ and Cl^- ions, resulting in the reduction of intracellular Cl^- level in the cells [40,47]. The measurement deviation on A549 and H1299 were also higher than SKOV3 and NP460 cells, but the deviation was smaller in FMD treatment than in the untreated and DMSO controls.

DMSO controls indicated slight changes in intracellular Cl^- and K^+ concentration influences intracellular K concentration through dissipation of ions, as DMSO is reported to be capable of inducing water pores formation and increasing the permeability of several ions, which may contribute to changes in intracellular ions composition [48,49]. Additionally, A549 and H1299 displayed higher overall intracellular Cl^- reading compared to the other 2 cells. This difference might be caused by the difference in cell media used to grow the cells or possibly stemmed from fundamental differences in intracellular Cl^- concentration due to the origin of cancers, which warrants future investigations.

On the other hand, FMD treatment seems to have no significant effects on intracellular K^+ measurement (Fig. 3). XRF measurement displayed no significant difference in measurement reading in all cell lines and through all treatments, signifying the drug cannot alter cells' intracellular K^+ level. The intracellular K^+ measurement displayed a higher deviation throughout all cell lines than intracellular Cl^-, but the average of the readings showed that the normal cell line has lower intracellular K^+ than the cancer cell lines. Furthermore, the 2 lung cancer cell lines, A549 and H1299, have the highest intracellular K^+, similar to the intracellular Cl^- reading.

3.3. Quantification of intracellular Cl^-

To assess the quantitative measurement accuracy, dried cells were spiked with a known amount of 5, 10 and 15 mM KCl solution and then freeze-dried. Cl spectra from each spiking concentration were used to calculate the linear regression graph. The graph demonstrated a linear increase in normalized Cl spectra with the higher spiked concentration, demonstrating high linearity of reading for Cl (R^2 = 0.992) (Fig. 4). Through the spiking test, we measured the LoD and LoQ of the XRF measurement for Cl^-. The measurement was based on the LoD and LoQ calculations reported by Chen *et al.* and displayed as follows [50]:

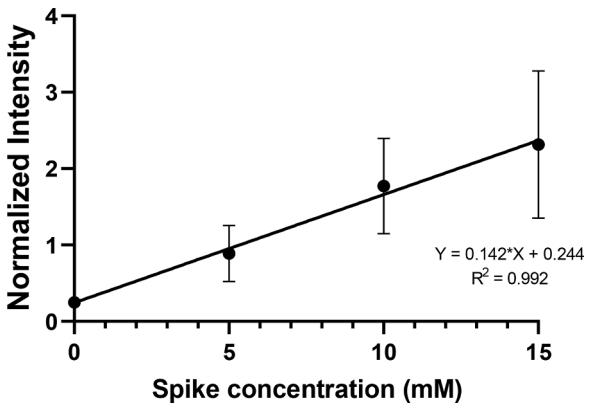

Fig. 4. XRF measurement result of KCl spike experiment. Untreated NP460 cells were dried and spiked with 5–15 mM KCl solution before being subjected to the second freeze-drying cycle. The linear regression curve for Cl was measured with XRF from all spike concentrations.

$$LoD = a \text{ x } 3SD + b$$

$$LoQ = a \text{ x } 10SD + b$$

With a and *b* are the intercept and slope of intracellular Cl^- linear regression graph and SD comes from the deviation of the respective peaks of Cl^- spectra in a blank dish. From the equations, the LoD and LoQ of Cl are 0.245 and 0.249 mM, respectively. Table 2 displays the intracellular Cl^- measurement of 4 different cell lines in untreated, DMSO control and FMD treatments from Figs. 2 and 3. The measurement could detect as low as 0.9 mM Cl^-, demonstrating the potentiality of combining the cell drying method and XRF analysis as a quantitative method for measuring intracellular Cl^- in adherent cells.

Table 1
Limit of Detection (LoD) and Limit of Quantitation (LoQ) of XRF measurement for Cl^-.

	Cl (mM)
LoD	0.245
LoQ	0.249

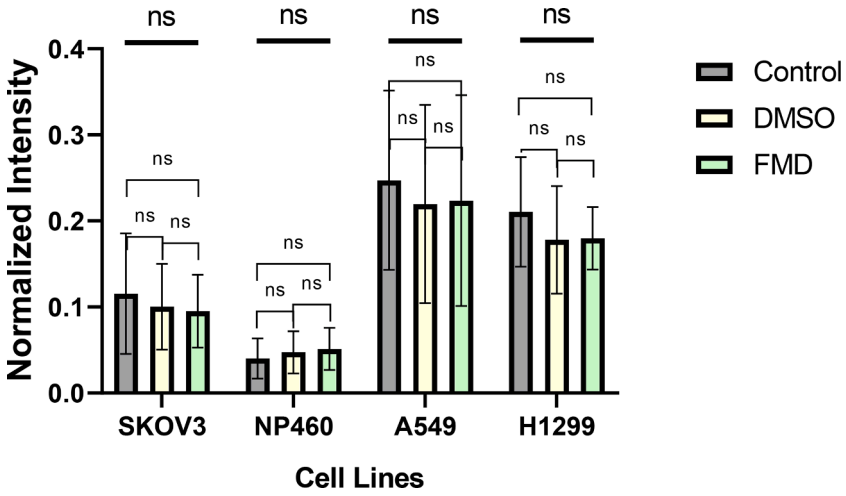

Fig. 3. XRF result of K measurement in dried cells with FMD treatment. Statistical tests were done with one-way ANOVA with Tukey's multiple comparison test. Ns: not significant.

Table 2
XRF measurement of intracellular Cl^- in dried cells.

Cell lines	Concentration of Cl− ions (mM)		
	Control	DMSO	FMD
SKOV3	1.296±0.274	1.345±0.379	0.935±0.216
NP460	1.591±0.317	1.300±0.321	0.961±0.326
A549	3.003±0.796	2.629±0.753	1.945±0.417
H1299	3.204±1.371	2.773±1.028	2.190±0.442

3.4. Single-cell EDS analysis

Single-cell EDS analysis on dried cells enables more direct testing of the elemental composition of individual cells (Fig. 5). The result is displayed as the mass fraction of weight (%Wt) of the corresponding element compared to the whole measured elements' weight. Since EDS measurement recorded all (%Wt) of the cell, Carbon (C) and Nitrogen (N) elements were excluded from the measurement due to the high proportion of carbon and nitrogen in form of carbohydrates, protein, nucleic acids and lipids constitutes 80 to 90% of cell's dry weight, which dwarfed the inorganic ions including K, Cl, Mg and Na that constitutes less than 1% of the dry weight [51]. EDS measured the following 5 elements: O, K, Cl, Na and Mg.

EDS analysis allowed a more precise measurement of Na^+ in the cell composition, which is not sensitive in XRF due to its lack of sensitivity towards lighter elements [52]. Though Na^+ can be detected in XRF [53, 54], its specific peak is small and hard to get clear peaks in biological samples where the Na^+ concentration is low.

EDS measurement on NP460 cells (Fig. 6A) displayed significant changes in all measured ions. DMSO and FMD treatment caused an increase (K^+) or decrease (Cl^- and Na^+) of dried cells' ion composition. On top of that, cells under DMSO control displayed a shift of intracellular ions compared to control cells, which indicated that DMSO alters the ion composition of the cells. Additionally, FMD treatment affected the intracellular ion, further increasing K^+ and reducing Na^+ and Cl^- in cells. The significant difference in ion composition of FMD-treated NP460 cells compared to other cells suggested that FMD influences changes in NP460 cell ion composition more than the other cell lines. Compared to the NP460 XRF result, the intracellular Cl^- fits with the XRF, although there is no significant change in DMSO-treated cells in Cl^-. As for potassium, the individual cell potassium fractional weight measured by EDS was increased in DMSO and FMD-treated cells. The increasing trend was also detected in the XRF measurement, albeit not a significant increase. This disparity could be caused by the sample number and the measurement area of these 2 methods. XRF measures thousands of cells in a wide area, while SEM-EDS measures a fraction of the area in single cells. Additionally, only 10 cells per treatment were tested in the SEM-EDS compared to thousands of cells measured in XRF.

Furthermore, EDS measurements on different regions of the dried cells displayed different weight ratios. Test on untreated NP460 cells measured in the center part of the cells (around the nuclei) and the periphery (Supp. Figure 2) gave a distinct result in weight ratio. Intracellular K^+ and Na^+ in the center were higher than the edge of the dried cells, while the intracellular Cl^- had no significant difference when measured from both locations (Supp. Figure 3). The effect on measurement location allows spatial analysis of the dried cells, which can generate the distribution of specific ion weight ratios within the cell.

On the other hand, a similar pattern on 3 measured elements is observed in SKOV3 cells. The Cl^- measured in EDS and XRF was reduced after FMD treatment (Fig. 6B). Na^+ composition is also reduced after FMD and DMSO treatment, suggesting that Na^+ and Cl^- ions are linked to the effect of the FMD drug. In the A549 cell line, EDS measurement showed no significant change in intracellular K^+ and Cl^-, while intracellular Na^+ was reduced (Fig. 6C). Meanwhile, H1299 cells do not show any changes in intracellular ions measured on all ions (Fig. 6D). There were variations in recorded results for each treatment across all measured ions, but none were statistically significant. As with the intracellular K^+ in NP460, the discrepancy in XRF and EDS results might be contributed by the same factors.

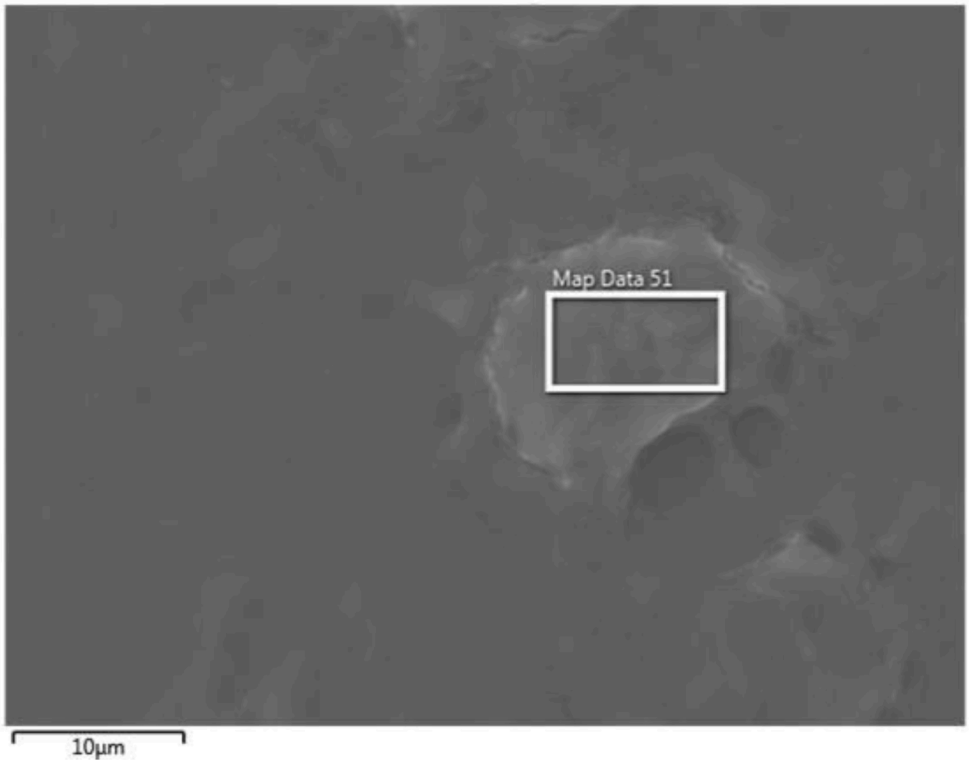

Fig. 5. Single-cell measurement of intracellular ions by SEM-EDS. Individual cells on the samples were measured by SEM-EDS to quantify the weight fraction of the ions in the dried cells.

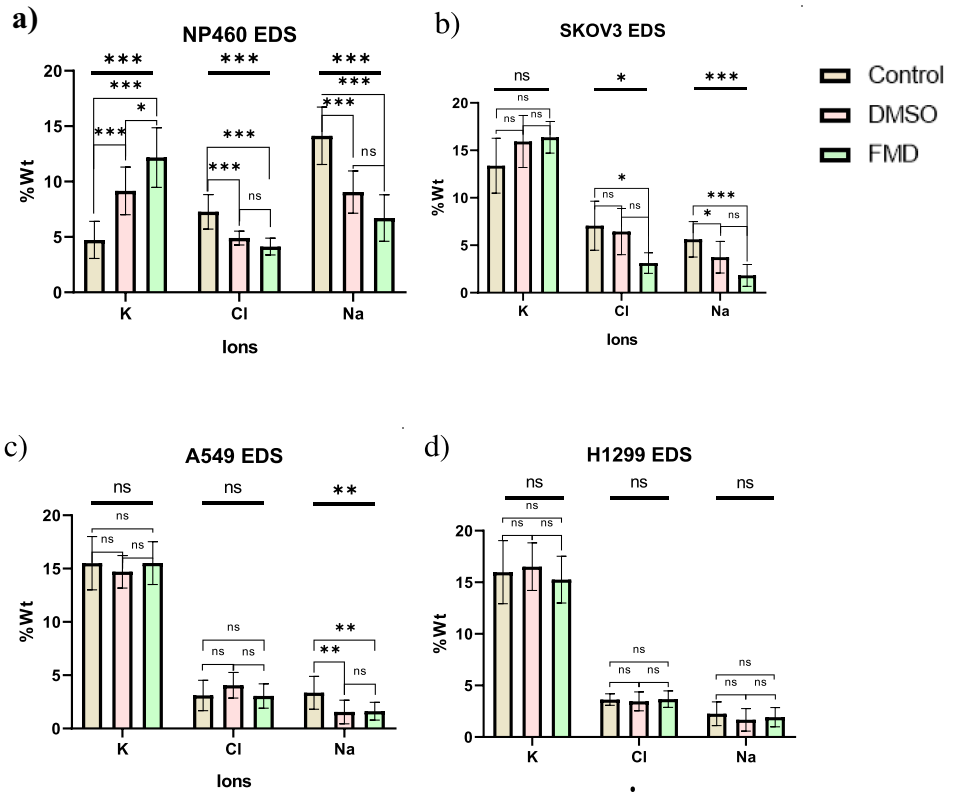

Fig. 6. Single-cell EDS analysis of K, Cl and Na elements on 4 different cell lines. Each element fractional mass (%Wt) is measured from single cells of 4 cell lines NP460 (A), SKOV3 (B), A549 (C) and H1299 (D). Statistical tests were done with ANOVA and Tukey's multiple comparison test. *: $P<0.05$, **: $P<0.01$, ***: $P<0.001$, ns: not significant.

The limitations in the intracellular Cl^- measurement proposed is the lack of established methods to measure in a single-cell resolution to validate the results. Prior reports in intracellular Cl^-measurement rely on self-calibration to validate their intracellular Cl^- measurement. Imaging-based measurement primarily conducted in situ analysis for calibration, a widely used method but still poses inaccuracies due to many uncontrolled variables during the process [19,28,55-57]. Similarly, analysis using ion-sensitive microelectrode involves calibration with Cl^- standard solutions [58,59]. Therefore, we performed a spiking analysis with Cl^- solution as a calibration step to validate the measured intracellular Cl^-.

DMSO has been reported to increase intracellular Ca^{2+} concentration by increasing cell membrane permeation, allowing extracellular Ca^{2+}ions to flood into the cytoplasm [49,60]. Though only increase in intracellular Ca^{2+}ions was reported, a similar mechanism could happen in changes in intracellular Na^+, K^+ or Cl^-. However, this effect is primarily observed in EDS results, as most XRF results showed no significant difference for DMSO control cells compared to FMD-treated cells. The variation in single-cell measurement might have been influenced by cell-to-cell heterogeneity, as cancer cells are heterogeneous and comprise subclusters of cells with different characteristics and metabolic rates [61,62].

The effect of FMD was reported previously in retinal and neuron cells, demonstrating a reduction of intracellular chloride activity in frog retina pigment epithelium (RPE) [63], rabbit and human ciliary epithelium (CE) [64], and gastric cancer cells, leading to slowing cancer cells proliferation [11]. Furthermore, FMD was reported to increase fractional sodium [39,65,66] and potassium [67] excretion in urine. Though the effect on intracellular concentration of Na^+ or K^+ was not directly experimented with, reduction in Na^+ and K^+ in the body could be related to changes in intracellular ion concentrations, as demonstrated in XRF and EDS measurements reported in this paper. However, further tests have to be performed to confirm this.

The reported freeze-drying method for intracellular ion measurement can preserve adherent cells for intracellular ion measurements but also have some technical limitations. XRF measurement for Cl^- has high sensitivity but difficulties to measure intracellular Cl^- on a single cell scale remain a challenging task. A 3D ion measurement via tomographic XRF allows spatial analysis of various ions in single diatom cell, including Cl^-. However, the process requires up to 36 h of measurement, with half of the time was spent in manual work, and further 7 h for data acquisition. The prolonged radiation exposure for data acquisition is not suitable for mammalian cells, and furthermore, additional correction algorithms is required for low atomic weight elements, making the application in mammalian cells sample limited [68,69]. SEM-EDS, while able to measure single cells, can only estimate the ions' weight fractions. However, with proper equipment such as synchrotron microXRF imaging [33,36,38], this method can be utilized for single cell measurement. Additionally, the wash with de-ionized water step may cause loss of intracellular ions, despite the short exposure and rapid freezing. The freeze-drying process might also cause small ruptures on the cell membrane after dehydration, which may contribute to intracellular ion loss. However, the staining test displayed that most cells retain their cytoplasmic and nucleus contents after freeze-drying, indicating that the loss might not be significant.

4. Conclusion

Our study demonstrates that the drying method employed to preserve the cells could retain the intracellular ions of the cells, preserving the intracellular ion and fixing the dried cells in place for detailed downstream analysis, such as single-cell level measurements. Drying the cells enables long-term preservation of samples without fear of sample degradation and enables tricky measurements such as intracellular ions

to be performed relatively cheaply and safely.

XRF measurement for intracellular Cl^- and K^+ demonstrated a linear result on incremental addition of spiked KCl, signifying an excellent quantitative capacity for Cl^- measurement in biological samples, able to detect Cl^- as low as 0.9 mM. Test on EDS displayed different patterns on some ions or cell lines compared to XRF, which may imply the heterogeneous nature of cancer cells within the populations of tested cells due to the difference in the amount of cells in XRF measurement and EDS measurement.

Meanwhile, treatment with the diuretic drug FMD reduced intracellular Cl^- across the cell lines. However, the effect on K^+ and Na^+ varies in different cell lines tested. Interestingly, some cell lines react to DMSO as well, possibly due to DMSO effect in increasing cell permeability, allowing transport of ions inside or outside the cells.

Declaration of Competing Interests

The authors declare that they have no known competing financial interests or personal relationships that could have appeared to influence the work reported in this paper.

Data availability

Data will be made available on request.

Acknowledgement

The work is supported by grant no. 7005507 from City University of Hong Kong. We would like to thank Prof. S.W. Tsao and C.M. Tsang for providing the NP460 cell line.

Supplementary materials

Supplementary material associated with this article can be found, in the online version, at doi:10.1016/j.talo.2023.100189.

References

[1] N. Pavillon, A. Benke, D. Boss, C. Moratal, J. Kühn, P. Jourdain, C. Depeursinge, P. J. Magistretti, P. Marquet, Cell morphology and intracellular ionic homeostasis explored with a multimodal approach combining epifluorescence and digital holographic microscopy, J. Biophotonics 3 (7) (2010) 432–436.
[2] M. Shekarabi, J. Zhang, A.R. Khanna, D.H. Ellison, E. Delpire, K.T. Kahle, WNK kinase signaling in ion homeostasis and human disease, Cell Metab. 25 (2) (2017) 285–299.
[3] M.J. Norris, M. Malhi, W. Duan, H. Ouyang, A. Granados, Y. Cen, Y.-C. Tseng, J. Gubbay, J. Maynes, T.J. Moraes, Targeting intracellular ion homeostasis for the control of respiratory syncytial virus, Am. J. Respir. Cell Mol. Biol. 59 (6) (2018) 733–744.
[4] Y. Wang, Y. Shi, H. Wei, Calcium dysregulation in Alzheimer's disease: a target for new drug development, J. Alzheimers Dis. Parkinsonism 7 (5) (2017) 374.
[5] F. Lang, C. Stournaras, Ion channels in cancer: future perspectives and clinical potential, Philos. Trans. R. Soc. Lond. B Biol. Sci. 369 (1638) (2014), 20130108.
[6] S.-H. Park, S.-.H. Park, E.N.W. Howe, J.Y. Hyun, L.-J. Chen, I. Hwang, G. Vargas-Zuñiga, N. Busschaert, P.A. Gale, J.L. Sessler, I. Shin, Determinants of ion-transporter cancer cell death, Chem 5 (8) (2019) 2079–2098.
[7] T.J. Jentsch, V. Stein, F. Weinreich, A.A. Zdebik, Molecular structure and physiological function of chloride channels, Physiol. Rev. 82 (2) (2002) 503–568.
[8] R. Wondergem, W. Gong, S.H. Monen, S.N. Dooley, J.L. Gonce, T.D. Conner, M. Houser, T.W. Ecay, K.E. Ferslew, Blocking swelling-activated chloride current inhibits mouse liver cell proliferation, J. Physiol. 532 (Pt 3) (2001) 661–672.
[9] B. Xu, J. Mao, L. Wang, L. Zhu, H. Li, W. Wang, X. Jin, J. Zhu, L. Chen, ClC-3 chloride channels are essential for cell proliferation and cell cycle progression in nasopharyngeal carcinoma cells, Acta Biochim. Biophys. Sin. (Shanghai) 42 (6) (2010) 370–380.
[10] D. Ye, H. Luo, Z. Lai, L. Zou, L. Zhu, J. Mao, T. Jacob, W. Ye, L. Wang, L. Chen, ClC-3 Chloride channel proteins regulate the cell cycle by up-regulating cyclin D1-CDK4/6 through suppressing p21/p27 expression in nasopharyngeal carcinoma cells, Sci. Rep. 6 (1) (2016) 30276.
[11] A. Shiozaki, E. Otsuji, Y. Marunaka, Intracellular chloride regulates the G(1)/S cell cycle progression in gastric cancer cells, World J. Gastrointest. Oncol. 3 (8) (2011) 119–122.
[12] K. Hiraoka, H. Miyazaki, N. Niisato, Y. Iwasaki, A. Kawauchi, T. Miki, Y. Marunaka, Chloride ion modulates cell proliferation of human androgen-independent prostatic cancer cell, Cellular Physiol. Biochem. 25 (4–5) (2010) 379–388.
[13] S. Kawai, T. Fujii, T. Shimizu, K. Sukegawa, I. Hashimoto, T. Okumura, T. Nagata, H. Sakai, T. Fujii, Pathophysiological properties of CLIC3 chloride channel in human gastric cancer cells, J. Physiol. Sci. 70 (1) (2020) 15.
[14] A. Yamagishi, F. Ito, C. Nakamura, Study on cancer cell invasiveness via application of mechanical force to induce chloride ion efflux, Anal. Chem. 93 (26) (2021) 9032–9035.
[15] H. Miyazaki, A. Shiozaki, N. Niisato, R. Ohsawa, H. Itoi, Y. Ueda, E. Otsuji, H. Yamagishi, Y. Iwasaki, T. Nakano, T. Nakahari, Y. Marunaka, Chloride ions control the G1/S cell-cycle checkpoint by regulating the expression of p21 through a p53-independent pathway in human gastric cancer cells, Biochem. Biophys. Res. Commun. 366 (2) (2008) 506–512.
[16] P. Bregestovski, T. Waseem, M. Mukhtarov, Genetically encoded optical sensors for monitoring of intracellular chloride and chloride-selective channel activity, Front. Mol. Neurosci. 2 (2009).
[17] T.B. Bolton, R.D. Vaughan-Jones, Continuous direct measurement of intracellular chloride and pH in frog skeletal muscle, J. Physiol. 270 (3) (1977) 801–833.
[18] R.F. Miller, R.F. Dacheux, Intracellular chloride in retinal neurons: measurement and meaning, Vision Res. 23 (4) (1983) 399–411.
[19] S. Kim, L. Ma, J. Unruh, S. McKinney, C.R. Yu, Intracellular chloride concentration of the mouse vomeronasal neuron, BMC Neurosci. 16 (1) (2015) 90.
[20] A. Sigaeva, Y. Ong, V.G. Damle, A. Morita, K.J. van der Laan, R. Schirhagl, Optical detection of intracellular quantities using nanoscale technologies, Acc. Chem. Res. 52 (7) (2019) 1739–1749.
[21] G. Rong, E.H. Kim, K.E. Poskanzer, H.A. Clark, A method for estimating intracellular ion concentration using optical nanosensors and ratiometric imaging, Sci. Rep. 7 (1) (2017) 10819.
[22] L. Ding, Y. Lian, Z. Lin, Z. Zhang, X.-D. Wang, Long-term quantitatively imaging intracellular chloride concentration using a core-/shell-structured nanosensor and time-domain dual-lifetime referencing method, ACS Sens. 5 (12) (2020) 3971–3978.
[23] N. Shcheynikov, A. Son, J.H. Hong, O. Yamazaki, E. Ohana, I. Kurtz, D.M. Shin, S. Muallem, Intracellular Cl^-as a signaling ion that potently regulates Na^+/$HCO3^-$transporters, Proc. Natl. Acad. Sci. 112 (3) (2015) E329–E337.
[24] K. Bomsztyk, M.B. Calalb, L. Smith, T.H. Stanton, A microelectrometric titration method for measurement of total intracellular Cl- concentration, Am. J. Physiol. 254 (1 Pt 1) (1988) C200–C205.
[25] J.R. Inglefield, R.D. Schwartz-Bloom, Confocal imaging of intracellular chloride in living brain slices: measurement of GABAA receptor activity, J. Neurosci. Methods 75 (2) (1997) 127–135.
[26] B. Pilas, G. Durack, A flow cytometric method for measurement of intracellular chloride concentration in lymphocytes using the halide-specific probe 6-methoxy-N-(3-sulfopropyl) quinolinium (SPQ), Cytometry 28 (4) (1997) 316–322.
[27] K.-I. Nakajima, Y. Marunaka, Intracellular chloride ion concentration in differentiating neuronal cell and its role in growing neurite, Biochem. Biophys. Res. Commun. 479 (2) (2016) 338–342.
[28] S. Sulis Sato, P. Artoni, S. Landi, O. Cozzolino, R. Parra, E. Pracucci, F. Trovato, J. Szczurkowska, S. Luin, D. Arosio, F. Beltram, L. Cancedda, K. Kaila, G.M. Ratto, Simultaneous two-photon imaging of intracellular chloride concentration and pH in mouse pyramidal neurons in vivo, Proc. Natl. Acad. Sci. U S A 114 (41) (2017) E8770–e8779.
[29] D. Arosio, G.M. Ratto, Twenty years of fluorescence imaging of intracellular chloride, Front. Cell. Neurosci. 8 (2014).
[30] J.-C. Chen, Y.-F. Lo, Y.-W. Lin, S.-H. Lin, C.-L. Huang, C.-J. Cheng, WNK4 kinase is a physiological intracellular chloride sensor, Proc. Natl. Acad. Sci. 116 (10) (2019) 4502–4507.
[31] K. Zia, T. Siddiqui, S. Ali, I. Farooq, M.S. Zafar, Z. Khurshid, Nuclear magnetic resonance spectroscopy for medical and dental applications: a comprehensive review, Eur. J. Dent. 13 (1) (2019) 124–128.
[32] T. Kagawa, S. Yoshida, T. Shiraishi, M. Hashimoto, D. Inadomi, M. Sato, T. Tsuzuki, K. Miwa, K. Yuasa, Basic principles of magnetic resonance imaging for beginner oral and maxillofacial radiologists, Oral Radiol. 33 (2) (2017) 92–100.
[33] A. Gräfenstein, C. Rumancev, R. Pollak, B. Hämisch, V. Galbierz, W.H. Schroeder, J. Garrevoet, G. Falkenberg, T. Vöpel, K. Huber, S. Ebbinghaus, A. Rosenhahn, Spatial distribution of intracellular ion concentrations in aggregate-forming HeLa cells analyzed by μ-XRF imaging, ChemistryOpen 11 (4) (2022), e202200024.
[34] S. Majumdar, J.R. Peralta-Videa, H. Castillo-Michel, J. Hong, C.M. Rico, J. L. Gardea-Torresdey, Applications of synchrotron μ-XRF to study the distribution of biologically important elements in different environmental matrices: a review, Anal. Chim. Acta 755 (2012) 1–16.
[35] M.J. Pushie, I.J. Pickering, M. Korbas, M.J. Hackett, G.N. George, Elemental and chemically specific X-ray fluorescence imaging of biological systems, Chem. Rev. 114 (17) (2014) 8499–8541.
[36] L. Yang, R. McRae, M.M. Henary, R. Patel, B. Lai, S. Vogt, C.J. Fahrni, Imaging of the intracellular topography of copper with a fluorescent sensor and by synchrotron x-ray fluorescence microscopy, Proc. Natl. Acad. Sci. U.S.A. 102 (32) (2005) 11179–11184.
[37] C. Körnig, T. Staufer, O. Schmutzler, T. Bedke, A. Machicote, B. Liu, Y. Liu, E. Gargioni, N. Feliu, W.J. Parak, S. Huber, F. Grüner, In-situ x-ray fluorescence imaging of the endogenous iodine distribution in murine thyroids, Sci. Rep. 12 (1) (2022) 2903.
[38] Q. Jin, T. Paunesku, B. Lai, S.-C. Gleber, S. Chen, L. Finney, D. Vine, S. Vogt, G. Woloschak, C. Jacobsen, Preserving elemental content in adherent mammalian

cells for analysis by synchrotron-based x-ray fluorescence microscopy, J. Microsc. 265 (1) (2017) 81–93.
[39] X. Huang, E.D. Mees, P. Vos, S. Hamza, B. Braam, Everything we always wanted to know about furosemide but were afraid to ask, Am. J. Physiol.-Renal Physiol. 310 (10) (2016) F958–F971.
[40] S.N. Orlov, S.V. Koltsova, L.V. Kapilevich, S.V. Gusakova, N.O. Dulin, NKCC1 and NKCC2: the pathogenetic role of cation-chloride cotransporters in hypertension, Genes Dis. 2 (2) (2015) 186–196.
[41] S. Somasekharan, J. Tanis, B. Forbush, Loop diuretic and ion-binding residues revealed by scanning mutagenesis of transmembrane helix 3 (TM3) of Na-K-Cl cotransporter (NKCC1), J. Biol. Chem. 287 (21) (2012) 17308–17317.
[42] K. Morishita, K. Watanabe, H. Ichijo, Cell volume regulation in cancer cell migration driven by osmotic water flow, Cancer Sci. 110 (8) (2019) 2337–2347.
[43] B.R. Haas, H. Sontheimer, Inhibition of the sodium-potassium-chloride cotransporter isoform-1 reduces glioma invasion, Cancer Res. 70 (13) (2010) 5597–5606.
[44] R. Gunawan, A. Imran, I. Ahmed, Y. Liu, Y. Chu, L. Guo, M. Yang, C. Lau, FROZEN! Intracellular multi-electrolyte analysis measures millimolar lithium in mammalian cells, Analyst 146 (16) (2021) 5186–5197.
[45] J.T.Y. Lee, K.L. Chow, SEM sample preparation for cells on 3D scaffolds by freeze-drying and HMDS, Scanning 34 (1) (2012) 12–25.
[46] M. Schu, E. Terriac, M. Koch, S. Paschke, F. Lautenschläger, D.A.D. Flormann, Scanning electron microscopy preparation of the cellular actin cortex: a quantitative comparison between critical point drying and hexamethyldisilazane drying, PLoS ONE 16 (7) (2021), e0254165.
[47] A.S. Jaggi, A. Kaur, A. Bali, N. Singh, Expanding spectrum of sodium potassium chloride Co-transporters in the pathophysiology of diseases, Curr. Neuropharmacol. 13 (3) (2015) 369–388.
[48] O. Trubiani, E. Salvolini, R. Staffolani, R. Di Primio, L. Mazzanti, DMSO modifies structural and functional properties of RPMI-8402 Cells by promoting programmed cell death, Int. J. Immunopathol. Pharmacol. 16 (3) (2003) 253–259.
[49] F. He, W. Liu, S. Zheng, L. Zhou, B. Ye, Z. Qi, Ion transport through dimethyl sulfoxide (DMSO) induced transient water pores in cell membranes, Mol. Membr. Biol. 29 (3–4) (2012) 107–113.
[50] Z. Chen, P.N. Williams, H. Zhang, Rapid and nondestructive measurement of labile Mn, Cu, Zn, Pb and As in DGT by using field portable-XRF, Environ. Sci. 15 (9) (2013) 1768–1774.
[51] G.M. Cooper, The Molecular Composition of Cells The Cell: A Molecular Approach, Sinauer Associates, Sunderland (MA), 2000.
[52] P. Brouwer, Theory of XRF: Getting Acquainted With the Principles, PANalytical B. V., Almelo, the Netherlands, 2003.
[53] J.A. Da-Col, M.I.M.S. Bueno, F.L. Melquiades, Fast and direct Na and K determination in table, marine, and low-sodium salts by X-ray fluorescence and chemometrics, J. Agric. Food Chem. 63 (9) (2015) 2406–2412.
[54] J.A. Stankey, C. Akbulut, J.E. Romero, S. Govindasamy-Lucey, Evaluation of X-ray fluorescence spectroscopy as a method for the rapid and direct determination of sodium in cheese, J. Dairy Sci. 98 (8) (2015) 5040–5051.
[55] J.V. Raimondo, B. Joyce, L. Kay, T. Schlagheck, S.E. Newey, S. Srinivas, C. J. Akerman, A genetically-encoded chloride and pH sensor for dissociating ion dynamics in the nervous system, Front. Cell Neurosci. 7 (2013) 202.
[56] M. Mukhtarov, L. Liguori, T. Waseem, F. Rocca, S. Buldakova, D. Arosio, P. Bregestovski, Calibration and functional analysis of three genetically encoded Cl (-)/pH sensors, Front. Mol. Neurosci. 6 (2013) 9.
[57] S.D. Watts, K.L. Suchland, S.G. Amara, S.L. Ingram, A sensitive membrane-targeted biosensor for monitoring changes in intracellular chloride in neuronal processes, PLoS ONE 7 (4) (2012) e35373.
[58] J.A. Heiny, S.C. Cannon, M. DiFranco, A four-electrode method to study dynamics of ion activity and transport in skeletal muscle fibers, J. General Physiol. 151 (9) (2019) 1146–1155.
[59] N.J. Klett, C.N. Allen, Intracellular chloride regulation in AVP+ and VIP+ neurons of the suprachiasmatic nucleus, Sci. Rep. 7 (1) (2017) 10226.
[60] H.M. Brown, B. Rydqvist, Dimethyl sulfoxide elevates intracellular Ca2+ and mimics effects of increased light intensity in a photoreceptor, Pflügers Archiv. 415 (4) (1990) 395–398.
[61] L. Keller, K. Pantel, Unravelling tumour heterogeneity by single-cell profiling of circulating tumour cells, Nat. Rev. Cancer 19 (10) (2019) 553–567.
[62] Y. Zhang, C. Guillermier, T. De Raedt, A.G. Cox, O. Maertens, D. Yimlamai, M. Lun, A. Whitney, R.L. Maas, W. Goessling, K. Cichowski, M.L. Steinhauser, Imaging mass spectrometry reveals tumor metabolic heterogeneity, iScience 23 (8) (2020), 101355.
[63] M. Wiederholt, J.A. Zadunaisky, Decrease of intracellular chloride activity by furosemide in frog retinal pigment epithelium, Curr. Eye Res. 3 (4) (1984) 673–675.
[64] T.C. Chu, R.R. Socci, M. Coca-Prados, K. Green, Comparative studies of furosemide effects on membrane potential and intracellular chloride activity in human and rabbit Ciliary epithelium, Ophthalmic Res. 24 (2) (1992) 83–91.
[65] M. Hropot, E. Klaus, R. Unwin, G. Giebisch, Diminished diuretic and natriuretic response to furosemide in potassium-depleted rats, Kidney Blood Pressure Res. 17 (1) (1994) 10–20.
[66] J.J. Beutler, W.H. Boer, H.A. Koomans, E.J. Dorhout Mees, Comparative study of the effects of furosemide, ethacrynic acid and bumetanide on the lithium clearance and diluting segment reabsorption in humans, J. Pharmacol. Exp. Therapeut. 260 (2) (1992) 768–772.
[67] C.E. Leonard, H. Razzaghi, C.P. Freeman, J.A. Roy, C.W. Newcomb, S. Hennessy, Empiric potassium supplementation and increased survival in users of loop diuretics, PLoS ONE 9 (7) (2014), e102279.
[68] M.D. de Jonge, C. Holzner, S.B. Baines, B.S. Twining, K. Ignatyev, J. Diaz, D. L. Howard, D. Legnini, A. Miceli, I. McNulty, C.J. Jacobsen, S. Vogt, Quantitative 3D elemental microtomography of *Cyclotella meneghiniana*at 400-nm resolution, Proc. Natl. Acad. Sci. 107 (36) (2010) 15676–15680.
[69] E. Malucelli, M. Fratini, A. Notargiacomo, A. Gianoncelli, L. Merolle, A. Sargenti, C. Cappadone, G. Farruggia, S. Lagomarsino, S. Iotti, Where is it and how much? Mapping and quantifying elements in single cells, Analyst 141 (18) (2016) 5221–5235.